25th ABCM International Congress of Mechanical Engineering
October 20-25, 2019, Uberlândia, MG, Brazil

COB-2019-0526
A SIMPLE APPROACH TO THE VORTICES SIMULATION FOR ELECTRO-OSMOTIC FLOW IN A NOZZLE

W. S. Bezerra
Universidade Federal da Grande Dourados, Faculdade de Ciências Exatas e Tecnologia, Dourados, MS, Brazil
wesleybezerra@ufgd.edu.br
A. Castelo
Universidade de São Paulo, Instituto de Ciências Matemáticas e de Computação de São Carlos, SP, Brazil
castelo@icmc.usp.br
A. M. Afonso
Faculdade de Engenharia da Universidade do Porto, Departamento de Engenharia Mecânica, Centro de Estudos de Fenómenos de Transporte (CEFT), Porto, Portugal
aafonso@fe.up.pt

Abstract. *Electro-osmotic flow was studied by using of numerical simulations in a nozzle. Flow through nozzles may be useful to performing fluid mixing. In this work, we propose a numerical approximation to perform vortex simulation which occur after the flow passes through the contraction in the nozzle. The motion of the charges in the solution is described by the Poisson-Nernst-Planck equations and we used the generalized finite differences to solve the numerical problem. Solutions for electro-osmotic flow were obtained for the Phan-Thien/Thanner model. Simulations for electro-osmotic flow were performed in a nozzle. Vortex formation was verified by take into account a punctual charge perturbation model. This perturbation was proposed in this work in order to operate on a particular neighborhood near the corners. The results are discussed.*

Keywords: *finite differences, electro-osmotic, nozzle*

1. INTRODUCTION

Channels with contractions and expansions are generally used when one is interested in mixing any solution in a microchannel. Some studies involving this topic have been published. For instance (Olsson *et al.*, 1997) studied the flow in a nozzle as a micropump element. Later, (Seitz and Heinzl, 2004) published the study of microfluidic device containing 32 nozzles. Further, (Ae and Yang, 2008) performed experiments in which the vortices formation was verified after the flow passes near the sharp corners. Other application topic is the prodution of bubbles, which can be controlled in a micro-mixing (Wang *et al.*, 2013). In fact, mixing efficiency depends on the type of flow. Therefore, it is very important to have total control of flow properties. Here the idea is trying to simulate the behavior of the fluid flow for this kind of geometry, with special attention to electrical effects near the corners. Physical description of these effects referring to the movement of the charges near the corners is very complex, but we can try in some way to find a coherent approximation linking the phenomenon to numerical simulation. As experimentally found by (Ae and Yang, 2008), near the corners there are fluctuations in zeta potential on the walls, causing velocity change in that neighborhood. Here, initially the proposal is to put on an external perturbation on the potential, which we will physically consider to be due to punctual charges located near the corners.

2. Governing equations

We are assuming the fluid incompressible laminar and isothermal flow. Moreover, here the treatment of the governing equations will be given in dimensionless form. Thus, in this text we will be referring to the dimensionless flow properties, then the governing equations that we desire to solve are given by:

$$\nabla \cdot \mathbf{u} = 0, \tag{1}$$

$$\frac{\partial \mathbf{u}}{\partial t} + \mathbf{u} \cdot \nabla \mathbf{u} = -\nabla p + \frac{1}{Re} \nabla^2 \mathbf{u} + \nabla \cdot \mathbf{S} + \mathbf{F}, \tag{2}$$

$$\mathbf{T} = \frac{2(1-\beta)}{Re}\mathbf{D} + \mathbf{S}, \tag{3}$$

where $\mathbf{u}$ is the velocity field, t is time, p is the pressure, $Re = \rho U H/\eta_0$ is the Reynolds number, U is the average velocity, H is the channel height, ρ the mass density and η_0 denotes the total shear viscosity $\eta_0 = \eta_s + \eta_p$. The rate of deformation tensor $\mathbf{D} = \frac{1}{2}\left(\nabla\mathbf{u} + (\nabla\mathbf{u})^T\right)$ and $\mathbf{T}$ is the elastic stress. The dimensionless solvent viscosity coefficient is given by $\beta = \frac{\eta_s}{\eta_0}$. The evolution in time of the polimeric stress tensor is related by

$$\frac{\partial\mathbf{T}}{\partial t} + (\mathbf{u}\cdot\nabla)\,\mathbf{T} - \left[(\nabla\mathbf{u})^T\cdot\mathbf{T} + \mathbf{T}\cdot\nabla\mathbf{u}\right] = \frac{1}{De}\mathbf{M}\,(\mathbf{T})\,, \tag{4}$$

where $De = \lambda U/H$ is the Deborah number and λ is the relaxation time of the fluid. Here we will be use a kernel conformation tensor and then determine the stress tensor. An alternative form to describe viscoelastic models is by using the conformation tensor, $\mathbf{A}$. In general the equation for $\mathbf{A}$ can be written as

$$\frac{\partial\mathbf{A}}{\partial t} + (\mathbf{u}\cdot\nabla)\,\mathbf{A} - \left[\mathbf{A}\nabla\mathbf{u} + \nabla\mathbf{u}^{\mathbf{T}}\mathbf{A}\right] = \frac{1}{De}\mathcal{M}(\mathbf{A}), \tag{5}$$

where $\mathcal{M}(\mathbf{A})$ is define according to the viscoelastic model.

One of interest subject is to solve the Eq. (4) - or Eq. (5) - for high values of Deborah number De. Numerical methods are unstable for certain critical values of De. In order to overcome such failure, Fattal and Kupferman proposed a reformulation of the differential constitutive equations into a equation for the matrix-logarithm of the conformation tensor. Extending the ideas proposed by (Fattal and Kupferman, 2004, 2005), (Afonso *et al.*, 2012) presented a generic kernel-conformation tensor transformation that allows apply various kernel functions to the matrix transformation, in which the evolution equation for $\Bbbk(\mathbf{A})$, can be expressed in its tensorial formulations as

$$\frac{\partial\Bbbk(\mathbf{A})}{\partial t} + (\mathbf{u}\cdot\nabla)\,\Bbbk(\mathbf{A}) = \mathbf{\Omega}\Bbbk(\mathbf{A}) - \Bbbk(\mathbf{A})\mathbf{\Omega} + 2\mathbb{B} + \frac{1}{De}\mathbb{M}, \tag{6}$$

where $\mathbb{B}$ and $\mathbb{M}$ are symmetric tensors constructed by the orthogonalization of the diagonal tensors. Thus, the HiG-Flow system solves Eq. (6) instead of Eq. (4). Considering a Newtonian fluid flow, the tensor $\mathbf{S}$ is null and the velocity and pressure are only updated at each step of time.

2.1 Phan-Thien/Tanner model

Here we are interested in use the PTT model to solve the constitutive equation and then determine the velocity field. For this model, the right hand side of the Eq. (4) can be written as:

$$\mathbf{M}\,(\mathbf{T}) = \frac{2(1-\beta)}{Re}\mathbf{D} - \left(1 + \frac{\varepsilon\, Re\, De}{1-\beta}\mathrm{tr}\,(\mathbf{T})\right)\mathbf{T} - \xi\, De\,(\mathbf{T}\cdot\mathbf{D} + \mathbf{D}\cdot\mathbf{T})\,. \tag{7}$$

The dimensionless parameter ε is related to the steady-state elongational viscosity in extensional flows and ξ is a parameter associated with the molecular slip. If ξ is null, the model reduces to the simplified PTT (sPTT). On the other hand if ξ is not null, there will be a non-zero second normal-stress difference in shear, leading to secondary flows in ducts having non-circular cross-sections, which is superimposed on the streamwise flow (Phan-Thien, 1978). In fact the right hand side for the conformation tensor Eq. (5)is given by

$$\mathcal{M}(\mathbf{A}) = \left(1 + \frac{\epsilon\, Re\, De}{1-\beta}\mathrm{tr}\,(\mathbf{S})\right)(\mathbf{I} - \mathbf{A}) - 2\xi\, De\,(\mathbf{B} - \mathbf{BA}). \tag{8}$$

In this way the equations of motion can be solved for the PTT model fluid flow. Therefor the electrical contribuition must be take into account for fully flow description. In the next section we will show how the electrical source term was obtained.

2.2 Electro-osmotic force

The schematic representation of electro-osmotic flow is show in Fig. 1. The applied potential along the axis of the channel provides the driving force necessary to occur the electro-osmotic flow. Due to the symmetry of the problem, the analyzis was shown for half of the channel, that is $0 \leq y \leq H$ taking the origin of coordinate system at the channel axis.

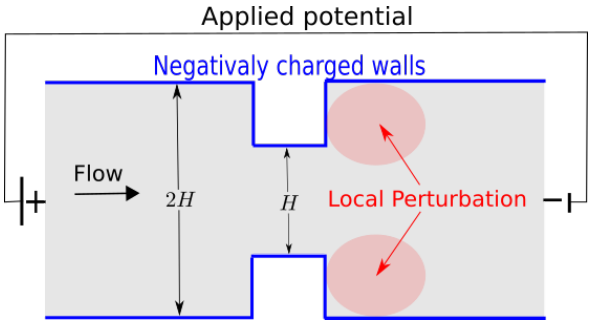

Figure 1. Scheme of electro-osmotic fluid flow in a nozzle. Disturbance occurs after the flow passing through contraction.

For the problems subjected to the electro-osmotic forces, there exists a source term in Eq. (2), $\mathbf{F} = \rho_e \mathbf{E}$, where $\mathbf{E}$ is the electric field. The electric field appears due to two contributions, one is the applied potential ϕ and the other due to the induced potential ψ which changes in the transversal direction to the channel walls. Thus, $\mathbf{E} = \nabla\phi + \nabla\psi$. The formation of the Debye layer occurs due to the spontaneous movement of the charged species near the channel wall, causing a charge redistribution in the fluid that originates the electrical double layer (Grahame, 1947). Therefore, the equations to be solved for these potentials are given by

$$\nabla^2\phi = 0, \tag{9}$$

$$\nabla^2\psi = -\rho_e, \tag{10}$$

where $\rho_e = \delta(n^+ - n^-)$ is the charge density, $\delta = n_0 e z H^2/\epsilon\zeta_0$ with n_0 the reference concentration, e is the elementary charge, z the charge valence, ϵ the dieletric constant and ζ_0 the potential on the wall. Moreover the density charge is related by n^+ and n^- which are respectivaly positive and negative ionic concentration. In this work we solve numerically the Nersnt-Planck equation for the ionic concentration:

$$\frac{\partial n^\pm}{\partial t} = -\mathbf{u}\cdot\nabla n^\pm + \frac{1}{Pe}\nabla^2 n^\pm \pm \frac{1}{Pe}\alpha\nabla\cdot\left[n^\pm\nabla(\phi+\psi)\right], \tag{11}$$

where $Pe = UH/D$ is the Peclet number that depends on ionic diffusion D. The potential to thermal energy ratio is given by $\alpha = ez\zeta_0/k_BT$ with k_B the Boltzmann's constant and T is the absolute temperature. The set of Eqs (9), (10) and (11) are solved to obtain the electrical force.

We are interested on the vortices formation in the nozzle. The proposal is to put on an external perturbation on the potential, which we will consider to be due to punctual charges located near the corners. Let us consider that the charges are very distant from each other, so we will be not take into account the isolated interaction by themselves. In addition, we consider that the interaction of the perturbation charges with the region before the contraction is negligible, assuming that the concentration of ions in this place remains stable, that is, the ionic depletions starts when the fluid arrives inside the contraction, where the ions feel intense electric gradient. It is known from the electromagnetism theory that the potential $\varphi(x,y)$ due to an elementary point charge is given by

$$\varphi(x,y) = \frac{Ke}{\sqrt{(x-x_0)^2+(y-y_0)^2}}, \tag{12}$$

where $P(x_0,y_0)$ is the place of the point charge is located, K is the dielectrical constant and e the elementary charge. In this way, the potential ψ_p on the walls near the cornners is the sum of reference zeta potential with perturbation potential, $\psi_p = \zeta_0 + \varphi$, and one can be write:

$$\psi_p = \zeta_0\left[1 + \frac{\omega}{\sqrt{(x-x_0)^2+(y-y_0)^2}}\right], \tag{13}$$

where we defined $\omega = KeH\nabla\phi/\zeta_0^2$ as a constant which depends on external applied field $\nabla\phi$, that is, increasing $\nabla\phi$, increases the electro-osmotic velocity and the perturbation effect on the standard potential ψ is consequently accentuated. On the other hand, increasing the distance from the wall, decreases the potential due the perturbation resulting $\psi_p \to \zeta_0$ from Eq. (13). By making $\psi_p = \psi_p^*\zeta_0$, $x = x^*H$ e $\omega = \omega^*H$, one can write the expression for dimensionless potential:

$$\psi_p^* = 1 + \frac{\omega^*}{\sqrt{(x^* - x_0^*)^2 + (y^* - y_0^*)^2}}. \tag{14}$$

According with (Probstein, 2005), the potential on the corners have a inverse square root of ionic concentration dependence, $\psi_p \sim n^{-1/2}$. In this way, the ionic concentration depends on inverse square of potential, lead to write the following relation:

$$n_p = n_{bc}\frac{\zeta_0^2}{\psi_p^2}, \tag{15}$$

where n_{bc} is the value of ionic concentration on the channel wall without perturbation effect. When ψ_p approaches the zeta potential, perturbation effects are negligible then the ionic concentration is given by $n_p = n_{bc}$. On the other hand, if ψ_p increases due the perturbation effect, then the ionic concentration decreases representing depletion of charges near the corners. Using the expression for ψ_p one can writing Eq. (15) in dimensionless form:

$$n_p^* = \frac{n_{bc}^*}{\left(1 + \dfrac{\omega^*}{\sqrt{(x^* - x_0^*)^2 + (y^* - y_0^*)^2}}\right)^2}. \tag{16}$$

For this proposal, the Eqs. (14) and (16) were implemented on the boundaries near the corners.

3. Computational procedures

The HiG-Flow/HiG-Tree system (Sousa *et al.*, 2018) was used to obtain numerical solutions reported in this work. Computational domain to the simulation is obtained through HiG-Tree compartment, which generates a hierarchical mesh. For bi-dimentional case, this mesh is a generalized quad-tree (Finkel and Bentley, 1974). Hierarchical meshes impose difficulties in the numerical scheme based on cartesian approximations, and requires the use of spatial interpolations at unknown points of the stencil. The interpolations of the properties in the center of the faces and in the center of the cells are made by the technique of moving least squares, which uses a given set of points where the property is known to estimate a unknown value in a neighbor point. Differential equations are discretized by the finite-differences method. Solvers using the PETSc library (Portable, Extensible Toolkit for Scientific Computation) (Balay *et al.*, 2017) are used to solve linear systems. The machine used to perform numerical simulations has a Core i7 2.0 GHz CPU, 16 Gb memory. The mesh with refinements along the channel were obtained using HiG-Tree. The total length of the mesh is $20H$. Near the walls the minimum size is $\Delta x_{min}/H = 6.250 \times 10^{-3}$. Figure 2 shows the mesh used to simulate the electro-osmotic flow in a nozzle. A typical simulation with dimensionless $\Delta t = 10^{-6}$, $Re = 10^{-3}$, $Pe = 10^{-2}$ and $De_\kappa = 2.0$ takes approximately one day.

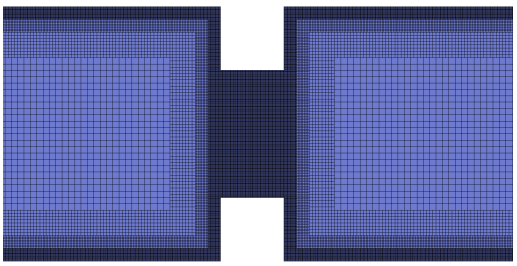

Figure 2. Illustration of the mesh to perform the electro-osmotic simulations in a nozzle. This mesh has 4 levels of refinement.

4. Results

Results are obtained for some perturbation values. We firstly show the images of flow properties in the nozzle.

Results provided by imposed perturbation are show in Figs 3-8. Figures 3 and 4 show the ionic concentrations n^+ and n^- respectivaly, in (a) for zero perturbation $\omega^* = 0.0$ and (b) for strong cornner effect by imposed $\omega^* = 0.006$, where accentuated changes on $n^\pm$ was observed. These changes are directly linked to the ψ changes and in fact occurs due to the coupling of Poisson-Nernst-Planck equations. The perturbation effect increases as ω^* is increased, as show in

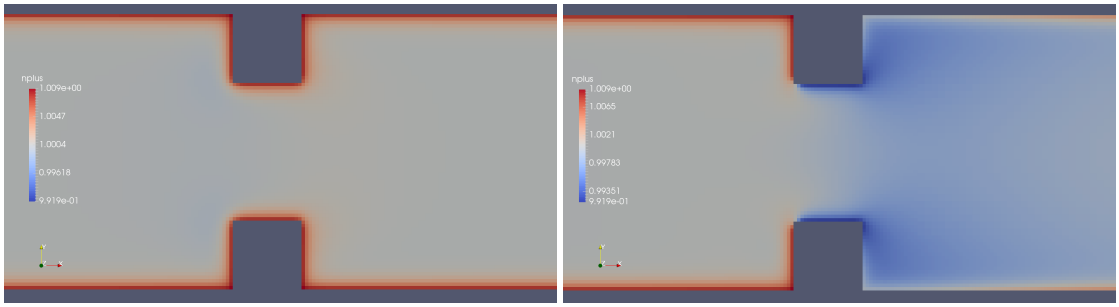

(a) (b)

Figure 3. Ionic concentration n^+. a) $\omega^* = 0.0$ and b) $\omega^* = 0.006$.

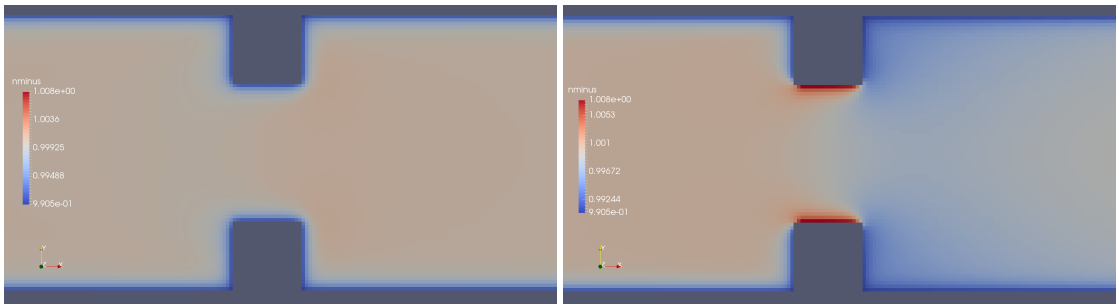

(a) (b)

Figure 4. Ionic concentration n^-. a) $\omega^* = 0.0$ and b) $\omega^* = 0.006$.

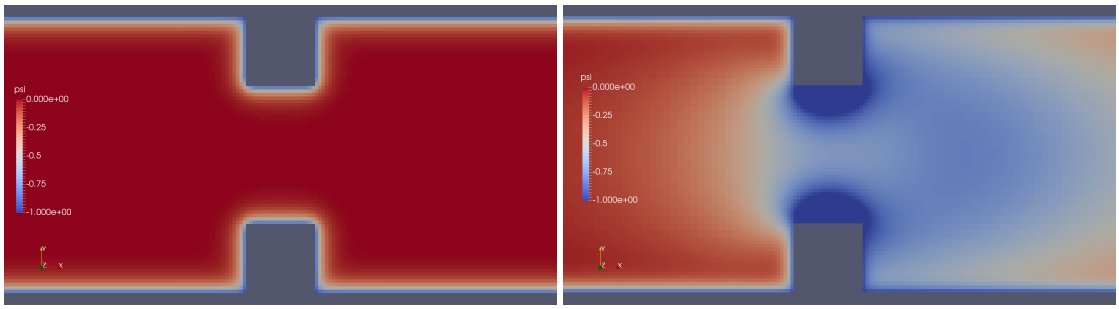

(a) (b)

Figure 5. Potential ψ. a) $\omega^* = 0.0$ and b) $\omega^* = 0.006$.

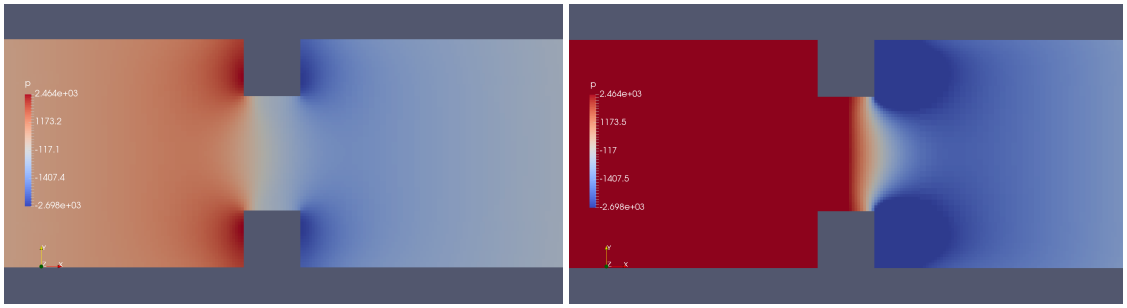

(a) (b)

Figure 6. Pressure p. a) $\omega^* = 0.0$ and b) $\omega^* = 0.006$.

Fig. 5. Therefor, the perturbation make changes on the pressure and velocity near the cornners as show in Figs. 6 and 7 . Increasing the perturbation parameter ω^*, the flow is concentrate in the center of the channel as show in Fig. 8, reducing the cross-section area of the fluid flow, contributing in the case of fluid mixing to be more efficiently process.

Figure 9 shows the curves of potential ψ as a function of the applied perturbation. For $\omega^* = 0$, there is no perturbation and the potential curves represented by squares are similar to that curve obtained for the parallel plate channel. The curves

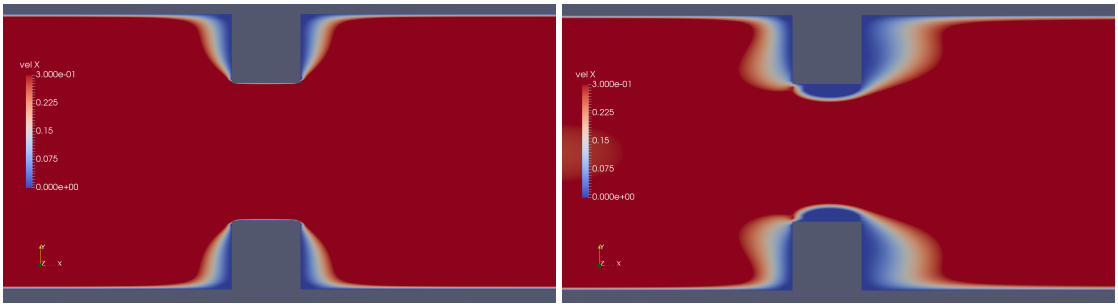

(a) (b)

Figure 7. Downstream velocity, in a) without perturbation, that is $\omega^* = 0.0$ and b) $\omega^* = 0.001$.

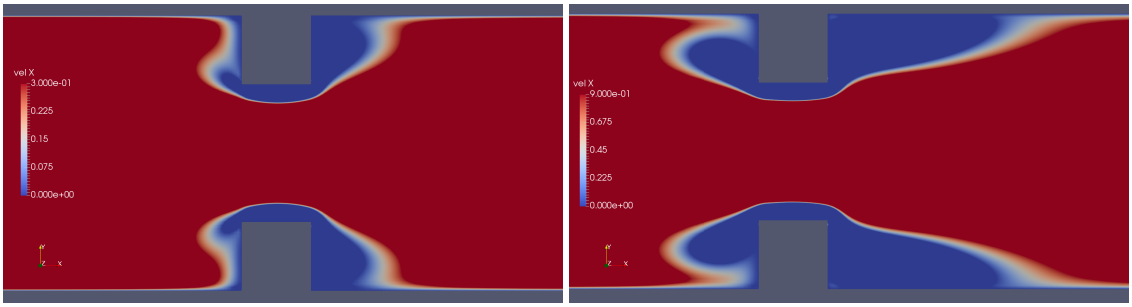

(a) (b)

Figure 8. Downstream velocity, in a) $\omega^* = 0.003$ and b) $\omega^* = 0.006$.

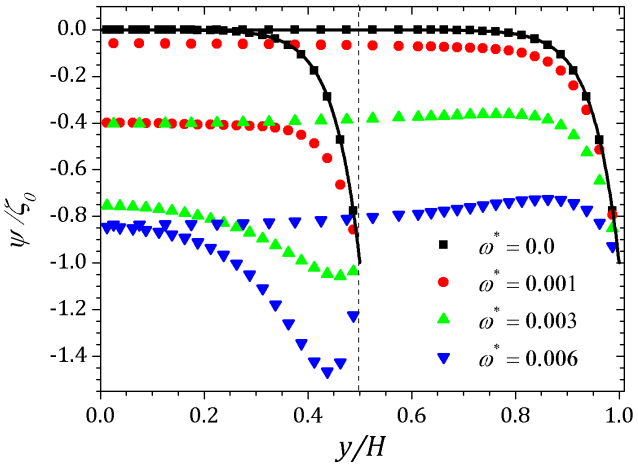

Figure 9. Potential ψ inside the contraction and right after the flow passes through it. Results for perturbation parameter $\omega^* = 0.0$, 0.001, 0.003 and 0.006.

represented by circles were imposing $\omega^* = 0.001$, then noticed an increase in the absolute value of ψ in the contraction and after the flow passing through it, and further up ψ approaches zero again indicating the decrease of perturbation effect out of the contraction. Increasing the perturbation parameter, $\omega^* = 0.003$ represented by up-triangles, can be seen an more accentuated increment in the potential within the contraction and out of it. For $\omega^* = 0.006$ represented by down-triangles, perturbation effect changes the potential to have approximately the same value in the plateau within the contraction and out of it.

The ionic concentration curves is shown in Fig. 10. For $\omega^* = 0$ represented by squares, the behavior is similar to the obtained for parallel plates channel. For $\omega^* = 0.001$ represented by circles, we observe a decrease in concentration n^+ and an increase of n^- within the contraction and this effect is smaller after the channel expansion. When $\omega^* = 0.003$ the concentration n^+ decreases while n^- increases and the curves are inverted relative to the reference concentration n_0, as shown in Fig. 11. This effect is even more pronounced for $\omega^* = 0.006$. In this way, the coupling between the potential

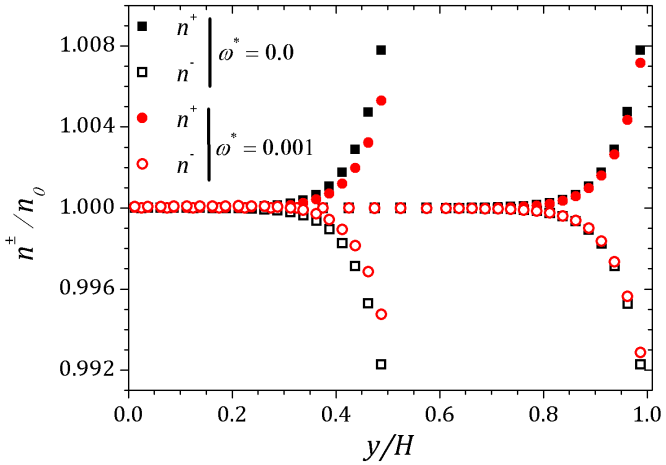

Figure 10. Ionic concentration $n^{\pm}$ inside the contraction and right after the flow passes through it. Results for perturbation parameter $\omega^* = 0.0$ and 0.001.

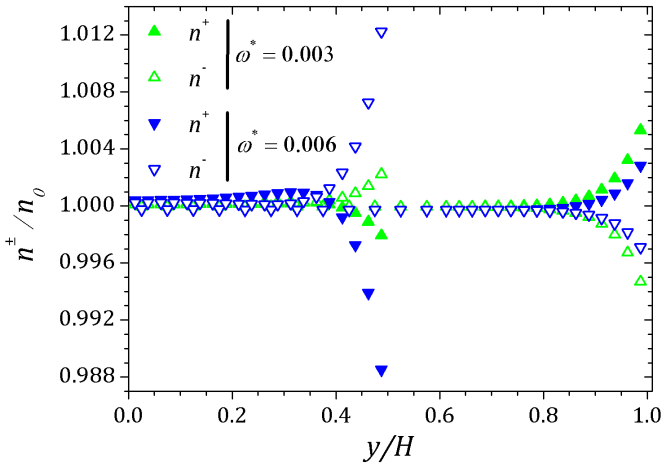

Figure 11. Ionic concentration $n^{\pm}$ inside the contraction and right after the flow passes through it. Results for perturbation parameter $\omega^* = 0.003$ and 0.006.

and ionic concentrations is related in Figs. 9, 10 and 11, indicating that the ionic concentration variation is affected by the potential increment due to perturbation. It is natural to expect that the perturbation imposed on the nozzle will cause numerical instabilities in the ionic concentration and potential ψ, since we are forcing a new distribution of charges for the problem, but if the perturbation is sufficiently small, the numerical method is stable. The velocity profiles are affected by both the perturbation and the variation of the pressure within the contraction. These curves were obtained at the center of the contraction and Fig. 12 shows the newtonian and viscoelastic profiles. The curves represented by squares correspond to $\omega^* = 0$, that is, velocity profile variations occur due to the variation of the pressure in the contraction, and tends to form a crest before to the velocity curve decay and then decreases until zero on the wall, where fully-squares correspond to the velocity for the Newtonian fluid. This effect is accentuated for the viscoelastic fluid, as can be seen in the curve represented by empty-squares. Increasing the perturbation effect, $\omega^* = 0.001$, the crests are suppressed as shown the curves represented by full and empty circles corresponding to the newtonian and viscoelastic fluid respectively. If $\omega^* = 0.003$ the profile forms a crest in the center of the channel and increases the distance from the center, so the velocity tends to zero quickly, as shown the curves with up-triangles. This effect is similar to the applying a pressure gradient on a parallel channel ends, as observed by (Afonso *et al.*, 2009). Finally, if $\omega^* = 0.006$, it is observed the existence of negative velocities near the wall, represented by the down-triangles. The polymeric tensor is shown in Figs. 13 and 14. These curves corroborates with the results obtained by (Afonso *et al.*, 2009) in order to show the similar effect to of applying a negative pressure gradient when the fluid enters in the contraction, represented by the fully points and a positive pressure gradient after the expansion of the channel represented by the empty points in graphic.

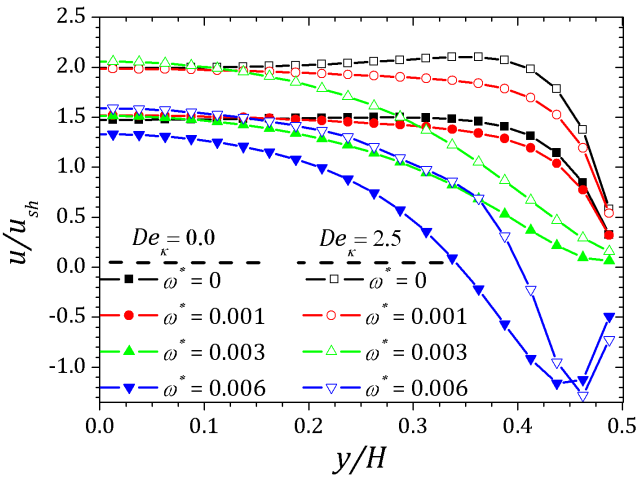

Figure 12. Perturbation effect on the velocity profile for sPTT model. Results for $De_\kappa = 2.5$, $\varepsilon = 0.1$ and perturbation parameter $\omega^* = 0.0$, 0.001, 0.003 and 0.006.

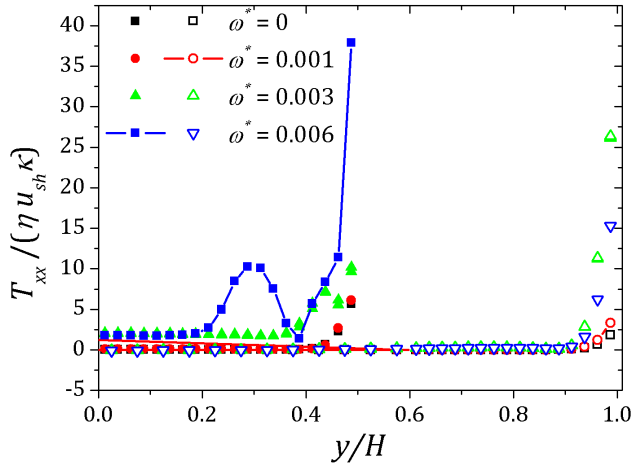

Figure 13. Normal stress inside the contraction and right after the flow passes through it. Results for $De_\kappa = 2.5$, $\varepsilon = 0.1$ and perturbation parameter $\omega^* = 0.0$, 0.001, 0.003 and 0.006.

5. Conclusions

Computational experiments were performed using the HiG-Flow system to obtain the solution of electro-osmotic flows. The sPTT model was used for viscoelastic flow simulation. Further, it was observed the vortex formation in a nozzle by imposed perturbation near the corners. This perturbation was adopted on some physical conditions and the results show similar behavior to the experiment performed by (Ae and Yang, 2008). The contraction in the channel naturally imposes a pressure gradient on that neighborhood. It was found that the imposed perturbation near the corners causes a similar effect. It is obvious that the imposition of the perturbation causes instabilities on the solution, as can be seen in the concentration results for the highest ω attempted. It is expected because one is imposing conditions unknown to the flow. However for weak perturbation the numerical solution keep stable.

6. ACKNOWLEDGEMENTS

W.S. Bezerra acknowledge the support by UFGD(Universideade Federal da Grande Dourados). A. Castelo thank the financial support from SÃčo Paulo Research Foundation (FAPESP) grant 2013/07375-0 and National Council for Scientific and Technological Development (CNPq) grants 307483/2017-7. A.M. Afonso acknowledge the support by CEFT (Centro de Estudos de Fenómenos de Transporte) and the funding by FCT (Fundação para a Ciência e a Tecnologia) through Project PTDC/EMS-ENE/3362/2014.

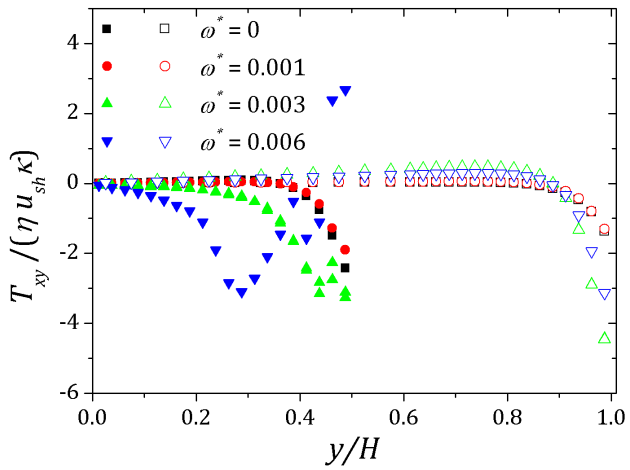

Figure 14. Shear stress inside the contraction and right after the flow passes through it. Results for $De_\kappa = 2.5$, $\varepsilon = 0.1$ and perturbation parameter $\omega^* = 0.0$, 0.001, 0.003 and 0.006.

7. REFERENCES

Ae, C. and Yang, R.J., 2008. "Vortex generation in electroosmotic flow passing through sharp corners". Vol. 5.

Afonso, A., Alves, M. and Pinho, F., 2009. "Analytical solution of mixed electro-osmotic/pressure driven flows of viscoelastic fluids in microchannels". *Journal of Non-Newtonian Fluid Mechanics*, Vol. 159, No. 1-3, pp. 50–63.

Afonso, A., Pinho, F. and Alves, M., 2012. "The kernel-conformation constitutive laws". *Journal of Non-Newtonian Fluid Mechanics*, Vol. 167, pp. 30–37.

Balay, S., Abhyankar, S., Adams, M.F., Brown, J., Brune, P., Buschelman, K., Dalcin, L., Eijkhout, V., Gropp, W.D., Kaushik, D., Knepley, M.G., McInnes, L.C., Rupp, K., Smith, B.F., Zampini, S., Zhang, H. and Zhang, H., 2017. "PETSc Web page". URL `http://www.mcs.anl.gov/petsc`.

Fattal, R. and Kupferman, R., 2004. "Constitutive laws for the matrix-logarithm of the conformation tensor". *Journal of Non-Newtonian Fluid Mechanics*, Vol. 123, No. 2, pp. 281–285.

Fattal, R. and Kupferman, R., 2005. "Time-dependent simulation of viscoelastic flows at high weissenberg number using the log-conformation representation". *Journal of Non-Newtonian Fluid Mechanics*, Vol. 126, No. 1, pp. 23–37.

Finkel, R.A. and Bentley, J.L., 1974. "Quad trees a data structure for retrieval on composite keys". *Acta Informatica*, Vol. 4, No. 1, pp. 1–9. ISSN 1432-0525. doi:10.1007/BF00288933. URL `https://doi.org/10.1007/BF00288933`.

Grahame, D.C., 1947. "The electrical double layer and the theory of electrocapillarity." *Chemical reviews*, Vol. 41, No. 3, pp. 441–501.

Olsson, A., Stemme, G. and Stemme, E., 1997. "Simulation studies of diffuser and nozzle elements for valve-less micropumps". In *Proceedings of International Solid State Sensors and Actuators Conference (Transducers' 97)*. IEEE, Vol. 2, pp. 1039–1042.

Phan-Thien, N., 1978. "A nonlinear network viscoelastic model". *Journal of Rheology*, Vol. 22, No. 3, pp. 259–283.

Probstein, R.F., 2005. *Physicochemical hydrodynamics: an introduction*. John Wiley & Sons.

Seitz, H. and Heinzl, J., 2004. "Modelling of a microfluidic device with piezoelectric actuators". *Journal of micromechanics and microengineering*, Vol. 14, No. 8, p. 1140.

Sousa, F.S., Lages, C.F.A., Ansoni, J.L., Castelo, A. and Simão, A., 2018. "A finite difference method with meshless interpolation for fluid flow simulations in non-graded hierarchical grids". *submetted to JCP*, Vol. vol, p. page.

Wang, S., Dhanaliwala, A.H., Chen, J.L. and Hossack, J.A., 2013. "Production rate and diameter analysis of spherical monodisperse microbubbles from two-dimensional, expanding-nozzle flow-focusing microfluidic devices". *Biomicrofluidics*, Vol. 7, No. 1, p. 014103.

8. RESPONSIBILITY NOTICE

The author(s) is (are) the only responsible for the printed material included in this paper.